NANO LETTERS

2005
Vol. 5, No. 11
2262−2267

Angle-Resolved Surface-Enhanced Raman Scattering on Metallic Nanostructured Plasmonic Crystals

Jeremy J. Baumberg,*,† Timothy A. Kelf,† Yoshihiro Sugawara,† Suzanne Cintra,‡ Mamdouh E. Abdelsalam,‡ Phillip N. Bartlett,‡ and Andrea E. Russell‡

School of Physics and Astronomy, and School of Chemistry, University of Southampton, Southampton, U.K.

Received August 16, 2005; Revised Manuscript Received September 26, 2005

ABSTRACT

Surface-enhanced Raman scattering is an ideal tool for identifying molecules from the "fingerprint" of their molecular bonds; unfortunately, this process lacks a full microscopic understanding and, practically, is plagued with irreproducibility. Using nanostructured metal surfaces, we demonstrate strong correlations between plasmon resonances and Raman enhancements. Evidence for simultaneous ingoing and outgoing resonances in wavelength and angle sheds new light on the Raman enhancement process, allowing optimization of a new generation of reproducible Raman substrates.

Raman scattering is a technique of great utility for identifying molecular species because a signature of re-emitted Raman photons is present for all molecular species and corresponds to a particular set of vibrational modes.[1] Unfortunately, only about one in every 10^{12} photons incident on a molecule undergoes Raman scattering making this technique, while powerful, applicable only in situations where large numbers of molecules are present. Thirty years ago it was discovered that Raman signals could be enhanced enormously by placing molecules close to a textured metal surface, raising the prospect of immediate broad application.[2] Unfortunately, to date this surface-enhanced Raman scattering (SERS) has proved to be of limited use, primarily because of the poor reproducibility of the enhanced signal. The origins of these enhancements are a topic of current debate: although commonly believed to have contributions from both electric field and chemical enhancement mechanisms[3,4] there is still uncertainty about what is crucial to form an "ideal" Raman enhancement substrate.

Recently, we have demonstrated a new form of nanostructured metal surface in which the plasmon modes can be engineered with great precision.[5,6] These plasmons correspond to localized electromagnetic fields that can be excited by incident light and can be confined strongly in the region of the metal surface. Such surfaces are distinguished from other SERS plasmon substrates by their smooth morphology and uniformity, and their void-like geometry giving reliably engineered plasmons. Plasmons have long been thought to be essential to the SERS process because of the effectiveness of the plasmon-active noble metals, such as Ag and Au, in producing large Raman signals.[7] Typical SERS substrates have generally consisted of electrochemically roughened Ag or flocculated Ag colloids, which give excellent enhancements but are generally extremely irreproducible. The enhancement is thought to be due to nanoscale "hot-spots" of tightly localized plasmons, which produce 1000-fold enhancements of the surface electromagnetic field.[8] These random hot-spots also account for the extreme variability of the surfaces, and their degradation when cleaning is attempted: the sharp nanoscale features that localize the plasmons are etched or deformed easily when the soft noble metals are chemically treated.

Here we show the power of plasmon engineering as a tool to systematically understand the SERS process and aid the design of optimal SERS substrates. A templating method is used to produce periodic arrays of spherical voids in metal films.[9,10] This geometry resembles the *inversion* of the metal dots or nanoparticles used for many recent SERS experiments.[11−13] Our voids or "antidots" are defined on a substrate rather than in solution, allowing ease of use as well as their integration into lab-on-chip systems. Furthermore, voids provide greater energy confinement than dots, hence giving greater surface enhancements.[5] Measuring the angle-resolved reflectivity of a "white-light" laser from nanostructured films allows the full spectral- and angular-dispersion of the plasmons to be mapped. Surface plasmons are electric field distributions pinned to a metallic surface. On a flat surface

* To whom correspondence should be addressed. E-mail: baumberg@phys.soton.ac.uk.
† School of Physics and Astronomy.
‡ School of Chemistry.

10.1021/nl051618f CCC: $30.25
Published on Web 10/15/2005

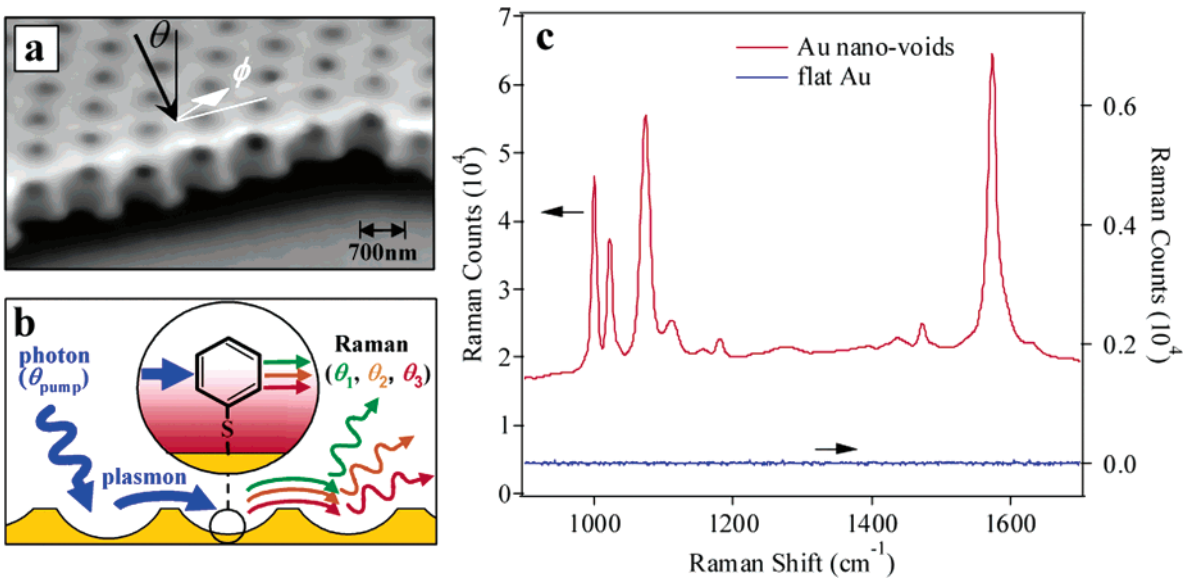

Figure 1. (a) Scanning electron micrograph of a sample a 90% sphere diameter ($\bar{t} = 0.9$), with definitions of θ and ϕ also shown. (b) Schematic SERS process; light is coupled into a plasmon, this then interacts and is Raman scattered by a molecule on the surface, and the outgoing plasmon is then scattered back into a photon. (c) SERS spectra taken using a Renishaw 2000 Raman System, 0.3 mW pump power at 633 nm with a 10-s integration time.

these pinned plasmons have too much momentum to be excited directly by incident light. However, a grating can be used to contribute extra momentum to the incident photons, allowing coupling into the surface plasmon polariton states (henceforth referred to simply as plasmons). When a surface is only weakly corrugated, propagating surface plasmons multiply scatter off the grating, and thus form plasmonic band gaps following typical Bragg dispersions.[14] However, when surfaces become strongly corrugated the plasmons become localized. For the spherical voids studied here, the localized plasmons resemble Mie modes of different spatial spherical harmonics.[15] By mapping the SERS signal at different angles of both the incident pump laser and the emitted Raman photons for the first time, we demonstrate clearly the resonant plasmon enhancement of the SERS signal. Sharp enhancements occur when the laser is scanned through a plasmon resonance (ingoing) and also when individual Raman scattered lines coincide with plasmon resonances (outgoing). We also show that ingoing and outgoing resonances can arise simultaneously from different plasmons. This demonstrates that SERS nanostructured substrates have to be carefully designed, and cannot be simply optimized by trial and error.

We use a combinatorial materials strategy to help identify the different plasmon and SERS regimes. Graded samples are grown with voids of different depths but of constant periodicity. The nanostructured surfaces are formed using a nanocasting process, by electrochemical deposition through a template of self-assembled latex spheres.[9,10] The resulting metallic mesh reflects the order of the self-assembled close-packed template, allowing convenient control of the pore diameters and regularity of the array. Templates are produced using a capillary force method, allowing a *monolayer* of well-ordered spheres to be produced: templates with sphere diameters, d, (and hence pitch) between 100 nm and several micrometers are produced successfully using this method. Electrodeposition while measuring the total charge passed allows accurate deposition of the metal to a required thickness, t. By systematically retracting the sample from the plating bath during growth, the nanostructure geometry can be graded. After deposition the template is dissolved, leaving the free-standing structure shown in Figure 1a. This allows the production of shallow, well-spaced dishes as well as almost encapsulated spherical voids on a single sample. Such nanostructures are considerably better defined than opaline structures that are infilled using chemical deposition. Optical and electron microscopy shows that the resulting surfaces are smooth on the 10-nm scale. We combine these with scanning-probe microscopy to determine the film thickness locally. To date, nanostructured metal films of gold, silver, nickel, cobalt, and platinum have all been realized. Here we concentrate on Au surfaces because of their chemical inactivity, although we have also demonstrated even stronger SERS enhancements for Ag voids.

The samples are mounted on an automated goniometer that allows the collection of both reflectance and SERS data; pump light is focused by a 30-cm focal length lens to a 100-μm spot on the sample. Reflectivity is measured using a supercontinuum white-light laser generated from ultrashort pulses;[16] this enables high angular resolution on a small sample area. The SERS signal is excited using up to 100 mW of a spectrally filtered tunable continuous wave Ti:sapphire pump laser. Spectra are collected through a separation spectral filter and focused into a multimode fiber that is coupled to a monochromator and cooled CCD. Only because the SERS enhancement is so high can we see scattered Raman photons from such a small numerical aperture (NA $\approx$ 0.001, roughly one hundred times smaller than that conventionally used in a Raman microscope). In contrast, standard Raman systems use large NA microscope objectives that average over the angular structure appearing in the measurements here. We observe no degradation of

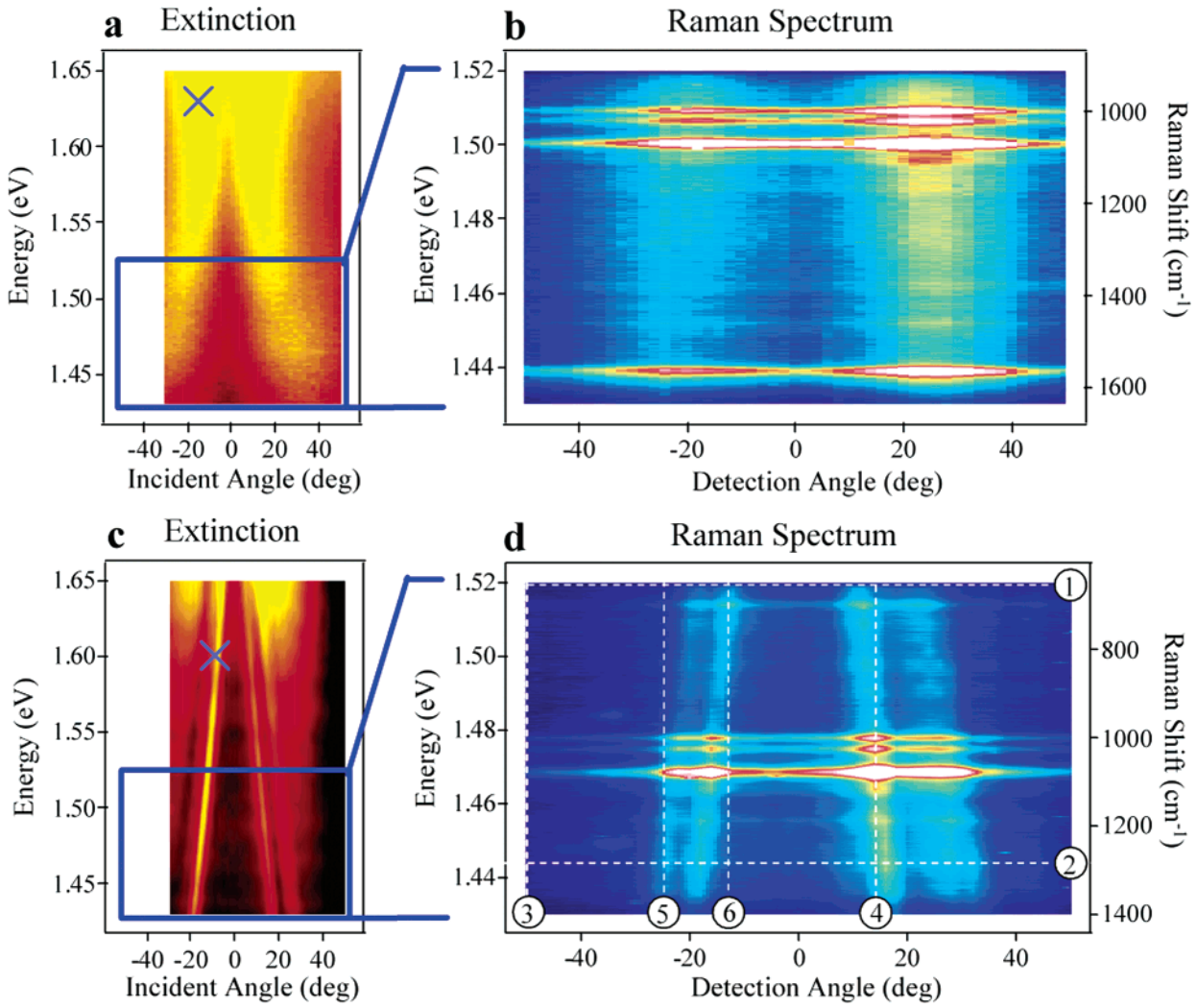

Figure 2. Extinction spectrum around the pump laser and Raman emission at different angles of incidence for (a) Au substrate containing 900-nm-diameter voids, at $\bar{t} = 0.5$. Bright regions correspond to stronger plasmon absorption. (b) SERS spectra for the same sample at different detection angles for a 760-nm pump at 16° (×). The integration time is 180 s, and the NA = 1×10^{-3}. Bright regions correspond to strong Raman signal. (c) Extinction from a Au 700-nm-diameter void substrate, at t = 0.2, and (d) Raman signal from this region, with a 775-nm pump at 7°, color scale same as in b.

the Raman signal after 12 h of continuous illumination, allowing many precise experiments to be performed at a single position. Spectra from different regions are also reproducible after at least 6 months of use and after numerous chemical cleanings. Measurements in a standard Raman confocal geometry confirm the enhancement factor from these gold surfaces to be $\sim 3 \times 10^6$, (uniformly distributed rather than in sporadic hot spots), which is consistent with factors reported elsewhere in the literature.[13]

Although previously unresolved for localized plasmons, SERS is supposed to consist of a five-step process (Figure 1b): (1) An ingoing photon interacts with the substrate exciting a plasmon. (2) The plasmon polarizes a molecule bound to the surface, creating a large effective dipole moment. (3) If the molecule now changes vibrational state, then its molecular polarization alters. (4) The change in molecular polarization couples back into an emitted *plasmon*. (5) Finally, the plasmon couples into an outgoing Raman scattered photon. The central advantage of SERS is that the plasmons improve the coupling between micrometer-scale photons and subnanometer molecules dramatically by acting as molecular antennae.[17] In the coupling process described above, the first and last steps should depend on the incident and detection angle, respectively.[18,19] Such an angular dependence would thus allow the identification of ingoing and outgoing plasmons and shed light on the plasmon-molecule coupling. To demonstrate the selectivity of the plasmon-SERS coupling, we use benzenethiol as a monolayer marker. Samples are cleaned in a bath of tetrahydrofluran, then soaked in a solution of benzenethiol in ethanol, and finally washed in ethanol to ensure a monolayer coverage of molecules on the surface. A typical SERS spectra is shown in Figure 1c, matching the expected spectrum from the literature.[20] We confirm monolayer coverage of benzenethiol from the absence of the C−S bond in the SERS spectra, as expected if all of these bonds are attached directly to the Au.[20,21] Knowing this coverage allows us to calibrate the Raman cross section per molecule.[22] To demonstrate the resonance conditions, we first map the reflectivity versus incident angle at a particular point on the sample, corre-

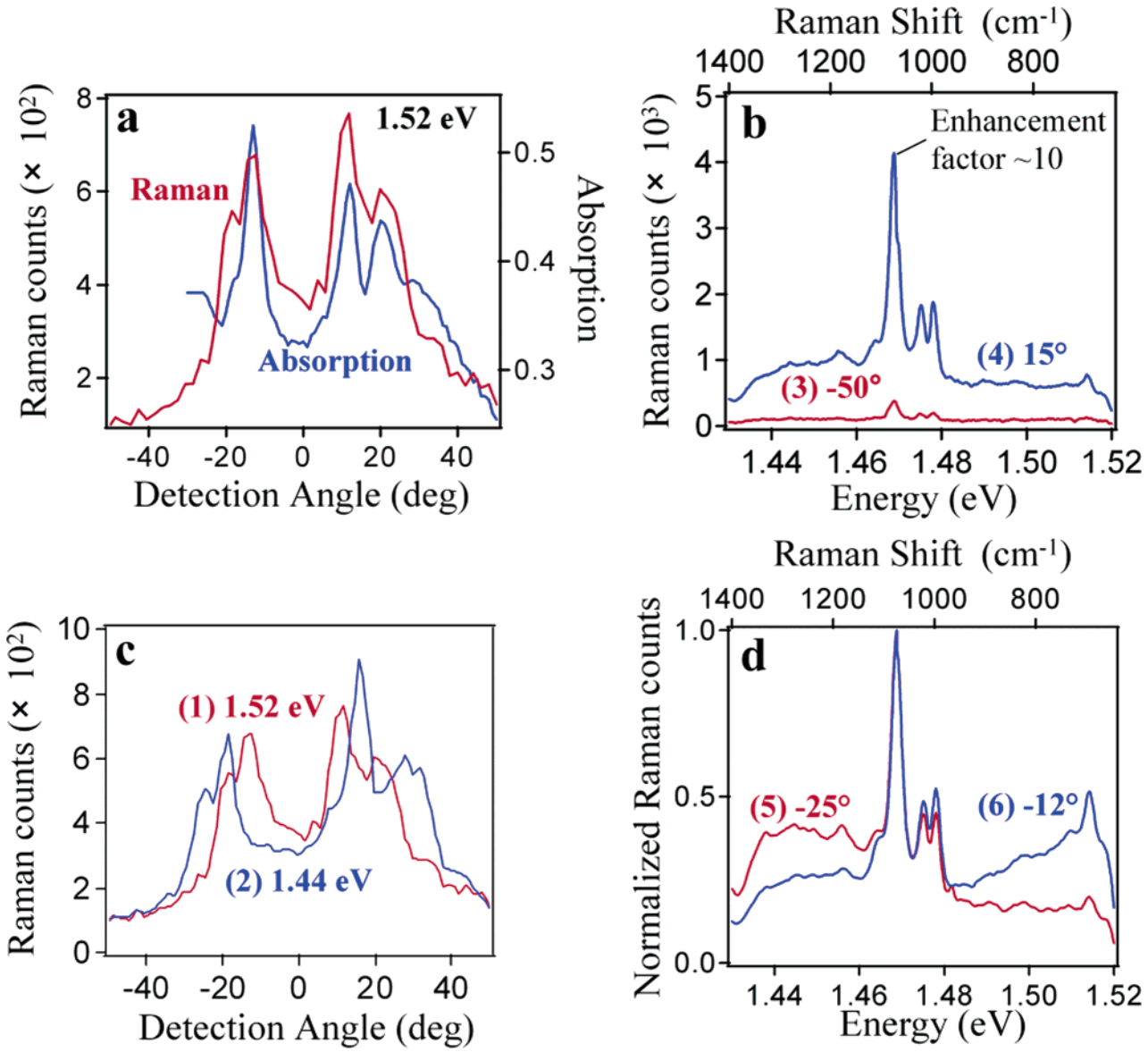

Figure 3. (a) Angle-resolved cross section through reflectivity and Raman spectra shown in Figure 2c and d at 1.52 eV, showing correlation between plasmon-related absorption in the reflectivity and Raman enhancement. (b) Raman spectra from sections 3 and 4 in Figure 2d; resonance with the plasmon enhances the signal by a factor of 10. (c) Cross sections 1 and 2 through Figure 2d show the different angle dependence of Raman intensity at different energies. (d) Raman spectra along sections 5 and 6 showing the different spectra seen at different observed angles (intensity normalized to the 1074 cm^{-1} peak).

sponding to a particular normalized void depth (Figure 2 a and c). Brighter points map stronger absorption by resonantly coupled plasmon modes.

From the extinction map, we can identify the plasmon type,[6] localized plasmons in the case of Figure 2a, and delocalized surface plasmons in Figure 2c. We first select a resonant pump angle (×) to coincide precisely with optimal absorption, and then collect SERS spectra at different detection angles (Figure 2b and d). Clear SERS lines are visible, which are enhanced at particular angles of detection. Thus the *outgoing* resonance of the plasmon-enhanced Raman scattering is identified here unambiguously. A weaker broadband background is also visible in the data, which is similarly enhanced by the plasmon modes. Although this background is ordinarily ignored it is clearly important, and a deeper discussion on the origins of the background is deferred to a future publication. Of key importance are the different SERS enhancements of different vibrational modes at different detection angles because of the dispersion of the plasmon energies with angle. This is more pronounced for the delocalized plasmon modes that possess stronger dispersion with angle.

Figure 3 shows a number of cuts through the data presented in Figure 2, and shows not only the strong angular dependence of the intensity of the SERS spectra but also their dependence on emitted photon energy. Slices taken through both the extinction and Raman data presented in Figure 2c and d give a direct correlation between the plasmons (which are observed as an increase in absorption) and the Raman enhancement. This correlation is demonstrated clearly in Figure 3a, providing evidence for the emission of Raman-scattered molecular polarization primarily

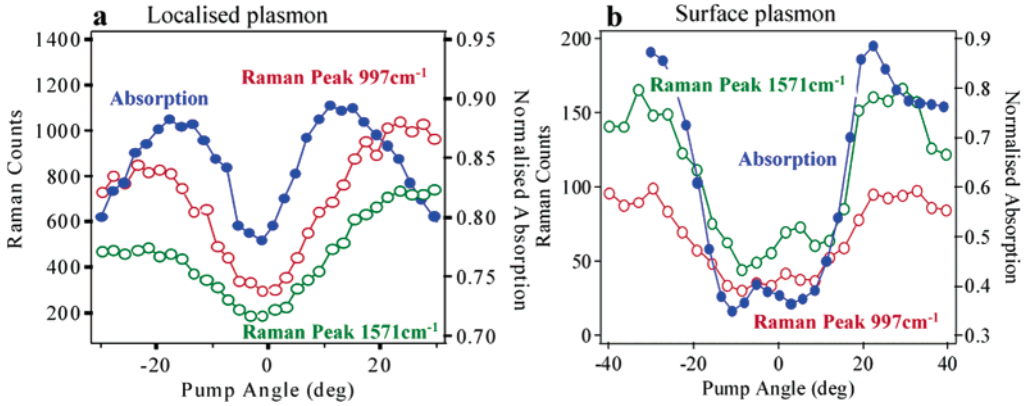

Figure 4. Angle-resolved cross section of the 997 cm^{-1} and 1574 cm^{-1} Raman peaks with changing incident pump angle. (a) Scanning through localized plasmon, detection angle equal to 23°. (b) Scanning through surface plasmon, detection angle equal to 15°.

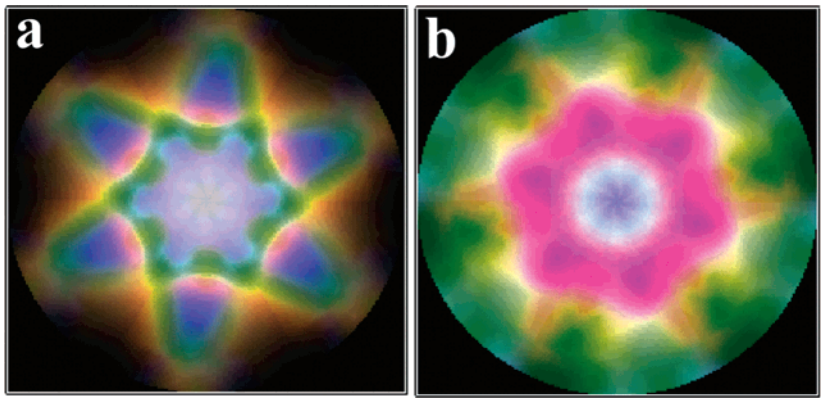

Figure 5. Emitted far-field Raman images deduced from the measured plasmonic nanovoid extinction for (a) propagating and (b) localized plasmons. Three vibrations have been included: 998 cm^{-1} (red), 1573 cm^{-1} (green), and 3055 cm^{-1} (blue). Pump laser at $\lambda = 600$ nm, sample has 900-nm-diameter voids, grown to a thickness of 220 nm (propagating) and 450 nm (localized). Images show incident angle, plotted radially, against sample orientation, plotted in the polar direction, as would be recorded in an image taken at the back of the collection microscope objective.

into plasmons before they are subsequently radiated, as in steps 4 and 5 of the model put forward in Figure 1b. Equivalent measurements on a substrate of electrochemically roughened Au show completely isotropic SERS emission, whereas no signal is obtained from flat Au. A simple grating effect cannot account for these observations because each Raman scattering event is not correlated in phase and cannot interfere in the far-field emission and also because the localized plasmons give the same resonant behavior as the delocalized surface plasmons. Interestingly, away from the plasmon resonance there is still a finite enhancement in the recorded Raman spectra (Figure 3b), which, although an order of magnitude below the on-resonance enhancement, is still many orders of magnitude above the enhancement from a control sample of flat Au grown using the same technique and whose Raman spectra cannot be resolved (Figure 1c). We believe that nonresonant SERS emission arises from molecules that are at sites with additional highly localized plasmons that have a broad range of energies and emit into all directions. Although these nanometer-localized plasmons absorb photons very weakly, molecules can Raman scatter into them more efficiently because of their small size and matched coupling. Thus, although the plasmon resonance gives the strongest contribution to the signal, it is not the only contribution.

This strong connection between plasmon modes and Raman emission is further emphasized in Figure 3c, which shows the variation in SERS intensity with detection angle for different detection energies. Although cuts through the background have been presented, this dependence holds equally true for different Raman lines. Different emission energies are enhanced at different detection angles, providing a systematic variation of the SERS spectra depending on the angle of viewing. This striking feature is shown directly in Figure 3d where simply changing the viewing angle alters the observed spectrum. Note that a conventional Raman microscope averages over a broad range of angles but in the cases presented here the majority of the enhancement occurs above ±20°, potentially outside a microscope's collection aperture. Hence, in order to use the relative intensities of the Raman lines to discuss molecular orientation and adduce molecular bonding, it is critical to understand and interpret SERS spectra in the light of the real plasmon dispersion.

To examine the ingoing resonance, we set the detection angle to one of the maxima for the outgoing resonance. The pump incident angle is then scanned while recording the SERS spectra (Figure 4). In this case, all of the outgoing Raman bands show the same enhancement, as expected from an ingoing resonance effect, depicted as steps 1 and 2 in

Figure 1b. Ingoing resonances are observed for both localized and surface plasmon modes.

The angular shape of the SERS enhancements observed for the ingoing and outgoing resonance scans are rather different, which naturally arises from the different angular-dispersion of the plasmons at the pump wavelength and the scattered Raman wavelength. Once again the weaker broad-band background is also enhanced in a similar way when the pump photon is maximally coupled to the plasmons. We note that all of the angular features in the above experiments are seen for a variety of plasmon resonances in a number of sample geometries, in which the height and diameter of the voids is changed. In addition, the samples show a SERS dependence on the sample azimuthal orientation for the delocalized plasmons (not shown), as expected from the hexagonally symmetric dispersion.[6] Also of great importance is the systematic repeatability of these observations, random hot spots are not observed and the quantitative reproducibility of 80 spectra taken at random positions over an approximately 0.5 cm^2 area show intensities with a deviation less than 10%.[22] Such SERS substrates, we believe, open the potential for effective application.

The angular beaming of plasmons observed here offers certain opportunities, in addition to the strong enhancements. Because the localized plasmon resonances can be tuned by our nanostructure design, the resonances can be pushed to regions of the spectrum (typically in the infrared) where luminescence is weak or absent in order to improve signal-to-noise in potential applications.[23] Another feature is that it allows the excitation and collection optics to be further spatially separated from the SERS substrate than is conventionally possible, thus allowing remote detection of trace molecules, for instance, in hazardous environments.

Another intriguing factor is the way the surface acts to beam different emitted frequencies in different directions. Figure 5 shows how plasmon modes of three distinct frequencies, corresponding to those of different Raman lines, depend on the incident angle (plotted radially) and azimuthal angle (plotted on the polar axis). This image thus corresponds to that within a Raman microscope at the back of the collection objective lens. The different frequencies are plotted in different colors and, because of the strong dispersion of the delocalized plasmon (and hence the SERS resonances), have very different appearances. By tailoring the plasmon dispersion, it should therefore be possible to concentrate the SERS signal into certain directions or to split different Raman peaks into different directions, or even turn off undesirable peaks. This technique could be utilized to produce a device capable of both enhancing and spectrally filtering the Raman spectra in one easy step.

With such a high degree of control over plasmon dispersions, as well as highly reproducible SERS spectra, there is hope that an improved understanding of the enhancement mechanisms can be progressed rapidly. Furthermore, a wide range of applications also becomes possible with reproducible Raman substrates including electrochemical control[24] and real-time monitoring of catalytic surface reactions, as well as environmental and security monitoring and clinical and pharmaceutical screening.

Acknowledgment. We acknowledge support from EPSRC Portfolio Partnership EP/C511786/1. Y.S. was supported by the JSPS fellowship for research abroad (Heisei 15).

References

(1) Schwartzberg, A. M.; Grant, C. D.; Wolcott, A.; Talley, C. E.; Huser, T. R.; Bogomolni, R.; Zhang, J. Z. *J. Phys. Chem. B.* **2004**, *108*, 19191.
(2) Fleischmann, M.; Hendra, P. J.; McQuillan, A. J. *Chem. Phys. Lett.* **1974**, *26*, 163−166.
(3) Moskovits, M. *Rev. Mod. Phys*. **1985**, *57*, 783−826.
(4) Otto, A. *Light Scattering in Solid IV, Topics in Applied Physics 54;* Springer-Verlag: Berlin, 1984.
(5) Coyle, S.; Netti, M. C.; Baumberg, J. J.; Ghanem, M. A.; Birkin, P. R.; Bartlett, P. N.; Whittaker, D. M. *Phys. Rev. Lett.* **2001**, *87*, 176801.
(6) Kelf, T. A.; Sugawara, Y.; Baumberg, J. J.; Abdelsalam, M.; Bartlett, P. N. *Phys. Rev. Lett*. **2005**, *95*, 116802.
(7) Tian, Z.-Q.; Ren, B.; Wu, D.-Y. *J. Phys. Chem. B.* **2002**, *106*, 9463−9483.
(8) Stockman, M. I.; Faleev, S. V.; Bergman, D. J. *Phys. Rev. Lett*. **2001**, *87*, 167401.
(9) Bartlett, P. N.; Birkin, P. R.; Ghanem, M. A. *J. Chem. Soc. Chem. Commun.* **2000**, 1671−3724.
(10) Bartlett, P. N.; Baumberg, J. J.; Coyle, S.; Abdelsalam, M. *Faraday Discuss.* **2003**, *125*, 19.
(11) Itoh, T.; Hashimoto, K.; Ikehata, A.; Ozaki, Y. *Appl. Phys. Lett.* **2003**, *26*, 5557−5559.
(12) Nie, S.; Emory, S. R. *Science* **1997**, *275*, 1102−1106.
(13) Dick, L. A.; McFarland, A. D.; Haynes, C. L.; Van Duyne, R. P. *J. Phys. Chem. B.* **2002**, *106*, 853−860.
(14) Barnes, W. L.; Dereux, A.; Ebbesen, T. W. *Nature (London)* **2003**, *424*, 824−830.
(15) Teperik, T. V.; Popov, V. V.; García de Abajo, F. J. *Phys. Rev. B.* **2005**, *71*, 085408.
(16) Netti, M. C.; Charlton, M. D. B.; Parker, G. J.; Baumberg, J. J. *Appl. Phys. Lett.* **2000**, *76*, 991−993.
(17) Baltog, I.; Primeau, N.; Reinisch, R.; Coutaz, J. L. *Appl. Phys. Lett.* **1995**, *66*, 1187−1189.
(18) Etchegoin P.; Cohen, L. F.; Hartigan, H.; Brown, R. J. C.; Milton, M. J. T.; Gallop, J. C. *J. Chem. Phys.* **2003**, *119*, 5281−5289.
(19) Kurosawa, K.; Pierce, R. M.; Ushioda, S. *Phys. Rev. B.* **1986**, *33*, 789−798.
(20) Szafranski, C. A.; Tanner, W.; Laibinis, P. E.; Garrell, R. L. *Langmuir* **1998**, *14*, 3570−3579.
(21) Han, S. W.; Lee, S. J.; Kim, K. *Langmuir* **2001**, *17*, 6981−6987.
(22) Cintra, S.; Abdelsalam, M. E.; Bartlett, P. N.; Baumberg, J. J.; Kelf, T. A.; Sugawara, Y.; Russell, A. E. *Faraday Discuss.* **2005**, *132*, 16.
(23) Kneipp, K.; Kneipp, H.; Itzkan, I.; Dasari, R. R.; Feld, M. S. *J. Phys.: Condens. Matter*. **2002**, *14*, R597−R623.
(24) Abdelsalam, M. E.; Bartlett, P. N.; Baumberg, J. J.; Cintra, S.; Kelf, T. A.; Russell, A. E. *Electrochem. Commun.* **2005**, *7*, 740−744.

NL051618F